Pressure Effect on Elastic Anisotropy of Crystals from Ab initio Simulations: The Case of Silicate Garnets.

A. Mahmoud, A. Erba, K. Doll, R. Dovesi
Pressure Effect on Elastic Anisotropy of Crystals from Ab initio Simulations: The Case of Silicate Garnets.
THE JOURNAL OF CHEMICAL PHYSICS (2014) 140

Pressure Effect on Elastic Anisotropy of Crystals from Ab initio Simulations: The Case of Silicate Garnets.

A. Mahmoud,[1] A. Erba,[1, a)] K. Doll,[2] and R. Dovesi[1]
[1)] *Dipartimento di Chimica and Centre of Excellence NIS (Nanostructured Interfaces and Surfaces), Università di Torino, via Giuria 5, IT-10125 Torino (Italy)*
[2)] *Institut für Elektrochemie, Universität Ulm, D-89081 Ulm, Germany*

(Dated: 3 April 2014)

A general methodology has been devised and implemented into the solid-state *ab initio* quantum-mechanical CRYSTAL program for studying the evolution under geophysical pressure of the elastic anisotropy of crystalline materials. This scheme, which fully exploits both translational and point symmetry of the crystal, is developed within the formal frame of one-electron Hamiltonians and atom-centered basis functions. Six silicate garnet end-members, among the most important rock-forming minerals of the Earth's mantle, are considered, whose elastic anisotropy is fully-characterized under high hydrostatic compressions, up to 60 GPa. The pressure dependence of azimuthal anisotropy and shear-wave birefringence of seismic wave velocities for these minerals are accurately simulated and compared with available single-crystal measurements.

I. INTRODUCTION

Modern seismology is a powerful tool for experimental measurements of the elastic properties of the Earth's deep interior whose outcomes provide essential information for discriminating among different compositional models of the crust, upper mantle and transition zone, once the elastic response of the individual constituents is well-characterized. In this respect, seismic data that are discussed by neglecting elastic anisotropy, can suggest models which are not correct.[1] Crystals of the mantle are generally anisotropic (olivine, the most abundant upper-mantle mineral, exhibits an average anisotropy of 24 %, for instance) and characterized by a relatively high degree of alignment due to typical mantle temperatures which allow for recrystallization. The effects of elastic anisotropy might be subtle and, among other manifestations, give usually rise to i) shear-wave birefringence that is, the two polarizations of transverse waves travel with different velocities, and ii) azimuthal anisotropy that is, the seismic wave velocities depend on propagation direction. If not properly recognized, anisotropic effects are generally modeled as inhomogeneities such as layering or gradients.

Silicate garnets are among the most important rock-forming minerals of the Earth's lower crust, upper mantle and transition zone. They are characterized by a cubic structure with space group $Ia\overline{3}d$ and formula $X_3Y_2(SiO_4)_3$, where the X site hosts divalent cations such as Ca^{2+}, Mg^{2+}, Fe^{2+} and Mn^{2+} and the Y site is occupied by trivalent cations such as Al^{3+}, Fe^{3+} and Cr^{3+}. At least twelve end-members of this family of minerals have been identified.[2] The primitive cell contains four formula units (80 atoms) and the structure consists of a network of corner-sharing SiO_4 tetrahedra and YO_6 octahedra. The most common end-members of the family are pyrope $Mg_3Al_2(SiO_4)_3$, almandine $Fe_3Al_2(SiO_4)_3$, spessartine $Mn_3Al_2(SiO_4)_3$, grossular $Ca_3Al_2(SiO_4)_3$, uvarovite $Ca_3Cr_2(SiO_4)_3$ and andradite $Ca_3Fe_2(SiO_4)_3$. Garnets are expected to play different roles in the Earth's mantle, depending on the particular geological model considered: in the pyrolite model[3] the entire upper mantle is chemically homogeneous and the garnet phase would be mainly composed by a pyralspite (pyrope-almandine-spessartine) solid solution; in the piclogite model[4,5] the transition region between 400 and 670 km depth would be richer in calcium and with more abundant garnets than the pyrolite model.

Some of us have recently illustrated how *ab initio* theoretical simulations do represent an effective and reliable tool for the investigation of various elastic properties of this class of materials: i) the elastic response of the six above-mentioned end-members has been computed at ambient pressure;[6,7] ii) elastic stiffness constants of pyrope, grossular and andradite have been computed at geophysical pressures up to 60 GPa;[8] iii) the elastic behavior of the *grandite* solid solution, $Ca_3Fe_{2-2x}Al_{2x}(SiO_4)_3$, has been explicitly computed as a function of its composition x.[9] In all cases, the theoretical description has been compared with available experimental data.[10–25]

In this paper, we apply *ab initio* theoretical simulations to the study of the evolution of elastic anisotropy of the six above-mentioned silicate garnet end-members under geophysical pressures. Furthermore, the elastic behavior of almandine, spessartine and uvarovite at high pressure is here addressed with *ab initio* techniques for the first time. Once the fourth rank elastic tensor has been computed, according to the elastic continuum theory, the three seismic wave velocities of a crystal, propagating along any direction, can be computed by solving Christoffel's equation[26,27] and can be labeled as quasi-longitudinal v_p, slow quasi-transverse v_{s1} and fast quasi-transverse v_{s2}, depending on their polarization with respect to the propagation direction.[28]

Calculations are performed with the CRYSTAL14

[a)] Electronic mail: alessandro.erba@unito.it

program[29,30] where some of the present authors and coworkers have implemented fully-automated and general procedures for computing elastic tensors under pressure, photoelastic constants and seismic velocities of crystals of any symmetry.[6,8,31–36] A fully periodic implementation of the global hybrid B3LYP, Becke-three parameters-Lee-Yang-Parr,[37,38] functional and all-electron basis sets are used.

The structure of the paper is as follows: In Section II the methodology adopted for the calculation of the elastic tensor of a crystal under pressure is briefly illustrated; the computational setup within which all calculations are performed is described in Section III; in Section IV we report and discuss the P-V relation of almandine, spessartine and uvarovite, along with the pressure dependence of seismic wave velocities and elastic anisotropy of the six end-members; conclusions are drawn in Section V.

II. THEORETICAL TECHNIQUE

A fully analytical scheme, based on the stress tensor, is used for optimizing the crystal volume associated with a given external pressure. The stress tensor $\boldsymbol{\sigma}$ is a symmetric second-rank tensor that can be computed analytically from the total energy density derivatives with respect to strain:

$$\sigma_{ij} = \frac{1}{V}\frac{\partial E}{\partial \epsilon_{ij}} = \frac{1}{V}\sum_{k=1}^{3}\frac{\partial E}{\partial a'_{ki}}a_{kj} \ , \qquad (1)$$

with $\boldsymbol{\epsilon}$ second-rank symmetric pure strain tensor and $i,j = x,y,z$. In the second equality, $\partial E/\partial \epsilon_{ij}$ has been expressed in terms of analytical energy gradients with respect to lattice parameters of the strained lattice, whose calculation has been implemented in the CRYSTAL program about ten years ago by Doll *et al.* for 1D, 2D and 3D periodic systems.[39,40] In the above expression, a_{ij} are elements of a 3×3 matrix, $\mathbf{A}$, where Cartesian components of the three lattice vectors $\mathbf{a}_1$, $\mathbf{a}_2$ and $\mathbf{a}_3$ are inserted by rows and V is the cell volume. When a distortion is applied to the cell, the lattice parameters transform as

$$a'_{ij} = \sum_{k=1}^{3}(\delta_{jk} + \epsilon_{jk})a_{ik} \ , \qquad (2)$$

where δ_{jk} is the Kronecker delta.

By adding an external hydrostatic "pre-stress" $\sigma_{ij}^{\rm pre} = P\delta_{ij}$ to σ_{ij} and by inverting equation (1), one gets the expression for the constrained gradients

$$\frac{\partial H}{\partial a_{ij}} = \frac{\partial E}{\partial a_{ij}} + PV(\mathbf{A}^{-1})_{ji} \ . \qquad (3)$$

Let us note that, with the inclusion of a hydrostatic pressure, the function to be minimized becomes the enthalpy $H = E + PV$. The implementation of a geometry optimizer under an external hydrostatic pressure, in the CRYSTAL program, has been done by Doll[41] so that the optimized volume V of any crystal at a given hydrostatic pressure P can be computed analytically.

In the absence of any finite pre-stress, elastic constants can be defined as second energy density derivatives with respect to pairs of infinitesimal Eulerian strains:

$$C_{ijkl} = \frac{1}{V_0}\left(\frac{\partial^2 E}{\partial \epsilon_{ij}\partial \epsilon_{kl}}\right)_{\epsilon=0} \ . \qquad (4)$$

An automated scheme for the calculation of the elastic tensor above has been implemented in the CRYSTAL program.[6,42]

If a finite pre-stress $\boldsymbol{\sigma}^{\rm pre}$ is applied in the form of a hydrostatic pressure P, within the frame of finite Eulerian strain, the relevant elastic stiffness constants read:[28,43–46]

$$B_{ijkl} = C_{ijkl} + \frac{P}{2}(2\delta_{ij}\delta_{kl} - \delta_{il}\delta_{jk} - \delta_{ik}\delta_{jl}) \ , \qquad (5)$$

provided that V_0 in equation (4) is replaced by the equilibrium volume $V(P)$ at pressure P. In the present, fully automated, implementation of the calculation of the stiffness tensor $\mathbf{B}$ (and of $\mathbf{S} = \mathbf{B}^{-1}$, the compliance tensor) under pressure, $V(P)$ is obtained from the analytical stress tensor described before. If Voigt's notation is used, according to which $v,u = 1,\dots 6$ ($1 = xx$, $2 = yy$, $3 = zz$, $4 = yz$, $5 = xz$, $6 = xy$),[47] the elastic stiffness tensor passes from a 4-index to a 2-index notation ($B_{ijkl} \rightarrow B_{vu}$) and, in general, exhibits, 21 independent elements that reduce to 3 (*i.e.* B_{11}, B_{12} and B_{44}) for crystals with cubic symmetry, as in the case of silicate garnets.

III. COMPUTATIONAL DETAILS

All the calculations reported in this manuscript are performed with the CRYSTAL14 program for *ab initio* quantum physics and chemistry of solid state.[30] The B3LYP one-electron Hamiltonian is adopted, which contains a hybrid Hartree-Fock/Density-Functional exchange-correlation term. All-electron atom-centered Gaussian-type-function (GTF) basis sets are adopted. Oxygen atoms are described by a (8s)-(411sp)-(1d) contraction of primitive GTFs, silicon by a (8s)-(6311sp)-(1d) one, aluminum by a (8s)-(611sp)-(1d) one, calcium by a (8s)-(6511sp)-(21d) one and magnesium by a (8s)-(511sp)-(1d) one. For iron, a (8s)-(64111sp)-(411d) contraction of GTFs is used, augmented with a further f-type polarization function as reported in detail in previous work.[48–50]

In CRYSTAL, the truncation of infinite lattice sums is controlled by five thresholds, which are set to 7 7 7 7 16.[29] Reciprocal space is sampled according to a sublattice with shrinking factor 3, corresponding to 4 points in the irreducible Brillouin zone. The DFT exchange-correlation contribution is evaluated by numerical integration over the cell volume: radial and angular points

of the atomic grid are generated through Gauss-Legendre and Lebedev quadrature schemes, using an accurate predefined pruned grid: the accuracy in the integration procedure can be estimated by evaluating the error associated with the integrated electronic charge density in the unit cell versus the total number of electrons per cell: $2 \times 10^{-5}|e|$ out of a total number of 800 electrons per cell for pyrope, for instance. The convergence threshold on energy for the self-consistent-field (SCF) step of the calculations is set to 10^{-10} hartree.

Equilibrium and strained configurations are optimized by use of analytical energy gradients calculated with respect to both atomic coordinates and unit-cell parameters or atomic coordinates only, respectively.[51–53] A quasi-Newtonian technique is used, combined with the BFGS algorithm for Hessian updating.[54–57] Convergence is checked on both gradient components and nuclear displacements; the corresponding tolerances on their root mean square are chosen to be 10 times more severe than the default values for simple optimizations: 0.00003 a.u. and 0.00012 a.u., respectively. For the elastic constants calculation, two strained configurations are considered for each independent strain, with a dimensionless strain amplitude of 0.01.

IV. RESULTS AND DISCUSSION

The first aspect to be discussed is the pressure-volume relation of the six silicate garnet end-members. In a recent investigation, we have computed the P-V relation for pyrope and grossular up to 60 GPa and for andradite up to 40 GPa with the same methodology described in Section II and compared it with available experimental studies.[8] For synthetic pyrope, a single-crystal X-ray diffraction study up to 33 GPa by Zhang *et al.*[58] was available, whereas a subsequent study by Zhang *et al.*[59] on synthetic single-crystal grossular and andradite up to 12 GPa and 14 GPa, respectively, was taken as a reference. The analytical stress tensor approach provided an excellent agreement with these experimental studies. An equation of state (EOS) approach was also investigated with four different analytical expressions (third-order Murnaghan's,[60] third-order Birch's,[61] logarithmic Poirier-Tarantola's[62] and exponential Vinet's[63]). When extrapolating to high pressure, the four EOSs slightly deviated from each other, still remaining relatively close to the analytical reference. On the contrary, we reported large deviations from the reference as regards the pressure dependence of the bulk modulus, the third-order Birch-Murnaghan providing the best description among them.

The P-V relation for almandine, uvarovite and spessartine is reported in Figure 1. Simulated data (as computed through the analytical stress tensor approach) are reported as continuous lines up to 6 GPa, 30 GPa and 40 GPa for almandine, uvarovite and spessartine, respectively. As main experimental reference, we consider

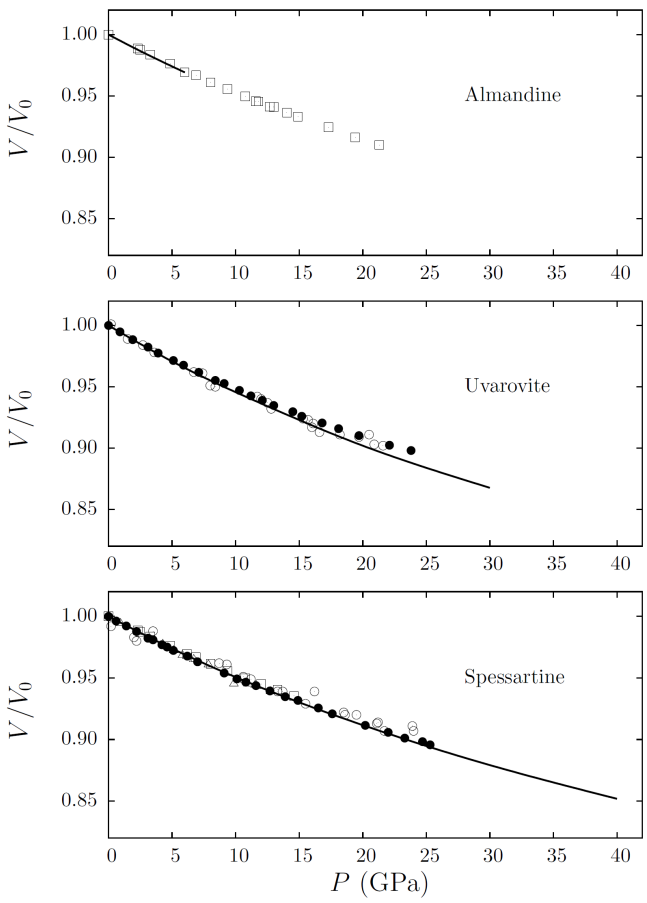

FIG. 1. V/V_0 is reported as a function of pressure P, for almandine (upper panel), uvarovite (middle panel) and spessartine (lower panel). Continuous lines represent computed values (with the analytical stress tensor scheme); full circles are experimental data from Ref. 64, open circles form Ref. 65, open squares from Ref. 59 and open triangles from Ref. 66.

the high-pressure X-ray synchrotron diffraction study of spessartine and uvarovite by Diella *et al.*[64] up to 25 GPa and 35 GPa, respectively (full circles). We also report the values obtained by Leger *et al.*[65] in their powder X-ray diffraction study as a function of pressure for spessartine and uvarovite up to 25 GPa (open circles). For almandine, single-crystal X-ray diffraction data by Zhang *et al.*[59], up to 22 GPa, are reported (open squares). Computed values for almandine are reported up to 6 GPa only because for higher pressures the electronic structure of the system is not converging within the numerical accuracy required by such calculations. For spessartine, other two compressional experiments are considered: a recent pressure-volume-temperature study by Gréaux *et al.*[66] up to 13 GPa (open triangles) and a single-crystal X-ray diffraction study by Zhang *et al.*[59] up to 15 GPa (open squares). The computed P-V relation for almandine and spessartine is found to be in excellent agreement with the accurate studies by Diella *et al.*[64] and Zhang *et*

TABLE I. Elastic properties of uvarovite (Uva), spessartine (Spe) and almandine (Alm) as a function of pressure P (GPa). Elastic stiffness constants B_{vu}, bulk modulus K_0, shear modulus $\overline{G}$, Young modulus E (expressed in GPa) and dimensionless Poisson's ratio σ are reported as computed at B3LYP level.

	P	B_{11}	B_{12}	B_{44}	K_0	$\overline{G}$	E	σ
Uva	0	306	83	87	158	96	240	0.25
	4	332	96	90	175	100	253	0.26
	8	356	110	93	192	104	264	0.27
	12	379	124	95	209	107	274	0.28
	20	419	151	99	240	112	290	0.30
	30	466	185	102	279	116	305	0.32
Spe	0	310	114	94	179	96	244	0.27
	4	334	126	98	195	101	258	0.28
	8	357	138	102	211	105	270	0.29
	12	380	151	106	227	109	282	0.29
	20	422	177	112	259	116	303	0.30
	30	472	210	119	297	123	325	0.32
	40	519	244	125	335	130	345	0.33
Alm	0	309	117	89	181	92	236	0.28
	2	322	123	92	189	95	245	0.28
	4	335	129	96	198	99	254	0.29
	6	347	136	99	206	102	262	0.29

al.[59] whereas for uvarovite the agreement is acceptable but somehow less satisfactory, particularly so when pressure exceeds 10 GPa.

According to the procedure described in Section II, we have computed the elastic stiffness constants B_{vu} of spessartine up to 40 GPa, of uvarovite up to 30 GPa and of almandine up to 6 GPa. The three independent constants, B_{11}, B_{12} and B_{44}, are reported in Table I as a function of pressure. When pressure increases, elastic stiffness constants increase with a quasi-linear behavior as previously observed for pyrope, grossular and andradite.[8] Let us discuss first spessartine and uvarovite for which we have computed elastic stiffness constants up to very high pressures: B_{12} shows the largest variation among them, changing by 123 % and 84 % passing from 0 to 30 GPa for uvarovite and spessartine, respectively; B_{11} changes by 52 % for both garnets, while B_{44} is found to be the least pressure dependent, varying by only 17 % and 27 %, respectively. To the best of our knowledge, no experimental data of elastic constants under pressure of spessartine and uvarovite have been reported so far. As regards almandine, experimental elastic constants under pressure have been reported by Jiang *et al.*[67] up to 11 GPa for an almandine-rich (72 %) garnet. The B_{11} constant increases by 12 % and 14 % from 0 to 6 GPa and from 0 to 5.8 GPa in our calculations and in the experiment, respectively, B_{12} by 16 % and 17 % and B_{44} by 11 % and 10 %, respectively. The overall agreement is definitely satisfactory.

We have computed high-pressure elastic properties of isotropic polycrystalline aggregates from the elastic stiffness and compliance constants through the Voigt-Reuss-Hill averaging scheme.[68,69] In particular, for cubic crystals, the adiabatic bulk modulus K_0 is simply defined as:

$$K_0 = \frac{1}{3}(B_{11} + 2B_{12}) \; . \tag{6}$$

The average shear modulus $\overline{G}$ can be expressed as:

$$\overline{G} = \frac{1}{10}(B_{11} - B_{12} + 3B_{44}) + \frac{5}{2}(4(S_{11} - S_{12}) + 3S_{44})^{-1} \; .$$

From the bulk modulus and the average shear modulus, expressions for Young's modulus E and Poisson's ratio σ can easily be obtained:

$$E = \frac{9K_0\overline{G}}{3K_0 + \overline{G}} \quad \text{and} \quad \sigma = \frac{3K_0 - 2\overline{G}}{2(3K_0 + \overline{G})} \; . \tag{7}$$

All these properties are reported in Table I as a function of pressure. Due to the fact that all these properties are derived from the elastic stiffness constants, they show a quasi-linear trend as a function of pressure too.

Most experimental studies of the elastic properties of garnets under pressure, report average seismic wave velocities.[15,25,67,70–73] Within the Voigt-Reuss-Hill scheme, the average values of quasi-transverse (shear), $\overline{v}_s$, and quasi-longitudinal, $\overline{v}_p$, seismic wave velocities can be computed as:[74]

$$\overline{v}_s = \sqrt{\frac{\overline{G}}{\rho}} \quad \text{and} \quad \overline{v}_p = \sqrt{\frac{K_0 + \frac{4}{3}\overline{G}}{\rho}} \; , \tag{8}$$

where ρ is the crystal density. We have simulated these seismic wave velocities for pyrope up to 60 GPa, for grossular, andradite, uvarovite and spessartine up to 30 GPa and for almandine up to 6 GPa, and reported them in Figure 2 (as continuous lines) where they are compared with available experimental data. It is clearly seen from Figure 2 that both $\overline{v}_s$ and $\overline{v}_p$ vary quasi-linearly with pressure, with $\overline{v}_s$ showing a smaller dependence on pressure than $\overline{v}_p$.

For pyrope, three accurate experiments have been performed at high pressure: a single-crystal Brillouin scattering study by Sinogeikin *et al.*[15] who reported values up to 20 GPa at ambient temperature (full circles); a synchrotron X-ray diffraction experiment by Gwanmesia *et al.*[70] up to 11 GPa at 300 K (open triangles) and an ultrasonic measurement at room temperature done by

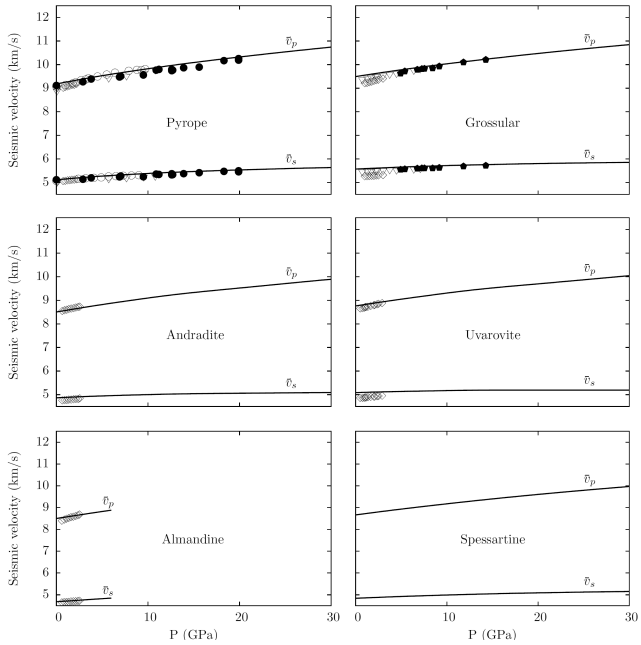

FIG. 2. Quasi-longitudinal, $\overline{v}_p$, and quasi-transverse, $\overline{v}_s$, average seismic wave velocities (in km/s) as a function of pressure P (in GPa) for pyrope, grossular, andradite, spessartine, uvarovite and almandine. Computed data are reported as continuous lines. Full circles are experimental data from Ref. 15, open circles form Ref. 71, open triangles from Ref. 70 and 72, full pentagons from Ref. 73 and open diamonds from Ref. 19.

Chen *et al.*[71] up to 10 GPa (open circles). For grossular, two reliable high-pressure synchrotron X-ray diffraction experiments by Gwanmesia *et al.*[72] (open triangles) and Kono *et al.*[73] (full pentagons) are reported up to 7 GPa and 14 GPa, respectively. As far as we know, no experimental data are available for spessartine. For andradite, uvarovite and almandine, the only available data are the low-pressure ones by Wang *et al.*[19] (open diamonds).

The overall agreement between our computed velocities and experimental ones is rather good, especially so when a comparison is possible with experiments at relatively high pressures. In particular, we note that the velocities measured by Wang *et al.*[19] for pyrope, grossular, andradite, uvarovite and almandine at very low pressures ($P < 3$ GPa) in most cases significantly deviate from other experimental datasets (when available) and computed values.

In principle, from accurate single-crystal Brillouin scattering experiments, directional seismic wave velocities can be measured which convey the essential information for analyzing into detail the elastic anisotropy of a crystal. However, few directional studies have been performed so far for silicate garnets.[15,25,67] From a fundamental point of view, within the elastic continuum model, the three acoustic wave velocities of a crystal, along any general direction represented by unit wave-vector $\hat{\mathbf{q}}$, can be related to the elastic constants by Christoffel's equation which can be given an eigenvalues/eigenvectors form as follows:[26,27]

$$\mathbf{A}^{\hat{\mathbf{q}}}\mathbf{U} = \mathbf{V}^2\mathbf{U} \qquad \text{with} \qquad A^{\hat{\mathbf{q}}}_{jk} = \frac{1}{\rho}\sum_{il} \hat{q}_i C_{ijkl} \hat{q}_l \ , \quad (9)$$

where $A^{\hat{\mathbf{q}}}_{jk}$ is Christoffel's matrix, ρ the crystal density, $i,j,k,l = x,y,z$ represent Cartesian directions, $\hat{q}_i$ is the i-th element of the unit vector $\hat{\mathbf{q}}$, $\mathbf{V}$ is a 3×3 diagonal matrix whose three elements give the acoustic velocities and $\mathbf{U} = (\hat{\mathbf{u}}_1,\hat{\mathbf{u}}_2,\hat{\mathbf{u}}_3)$ is the eigenvector 3×3 matrix where each column represents the polarization $\hat{\mathbf{u}}$ of the corresponding eigenvalue. The three acoustic wave velocities, also referred to as seismic velocities, can be labeled as quasi-longitudinal v_p, slow quasi-transverse v_{s1} and fast quasi-transverse v_{s2}, depending on the polarization direction $\hat{\mathbf{u}}$ with respect to wave-vector $\hat{\mathbf{q}}$.[28]

As we shall show in what follows, from the analysis of directional seismic wave velocities, the main aspects of elastic anisotropy, such as shear-wave birefringence and azimuthal anisotropy, can be fruitfully discussed, in particular as regards their evolution on pressure. In Figure 3 we report our computed directional seismic wave velocities for grossular, uvarovite, spessartine, pyrope, andradite and almandine along the same azimuthal angle θ which spans the (110) plane of the lattice by exploring all the most symmetric crystallographic directions: $\theta = 0°$ corresponds to the crystallographic direction [110], $\theta = 45°$ to [111] direction, $\theta = 90°$ to [001] direction, etc. Computed velocities are reported as continuous lines of increasing thickness as a function of pressure (0 GPa, 4 GPa, 8 GPa, 12 GPa, 20 GPa, 30 GPa). Available directional experimental data are also reported in the figure: for andradite, data from an accurate single-crystal Brillouin scattering experiment by Jiang *et al.*[25] are reported at ambient pressure (full squares) and at 8.7 GPa (full circles); a subsequent study by Jiang *et al.*[67] on a single-crystal grossular-rich garnet at 4.3 GPa (full circles) is also taken as a reference; for pyrope, data from the study by Sinogeikin and Bass[15] are reported. From comparison with available experiments, it is clearly seen how accurate the theoretical description of angular dependence, oscillation amplitudes and pressure shift of the seismic wave velocities can be.

From the analysis of Figure 3 we can sort the six end-members according to increasing propagation velocity, at zero pressure, as follows: Alm < And < Spe < Uva < Pyr < Gro; we can also notice that the sequence remains unchanged even under increasing pressure. Almandine shows the slowest v_p, while pyrope and grossular allow for the fastest propagation. In our previous work,[6] this behavior has been explained in terms of the elemental composition of the end-members via equation (8) which states that seismic wave velocities are inversely proportional to the density of the material. Fe-bearing phases, such as andradite and almandine are the most dense, followed by the Mn- and Cr-bearing phases, such as spessartine and uvarovite whereas pyrope and grossular contain the lightest elements (Mg, Ca) thus being the least dense

TABLE II. Computed average polycrystalline isotropic quasi-longitudinal, $\overline{v}_p$, and quasi-transverse, $\overline{v}_s$, seismic wave velocities (in km/s) and elastic anisotropy index (in %) as a function of pressure (in GPa) for pyrope, grossular, andradite, spessartine, uvarovite and almandine.

P	Pyrope			Grossular			Andradite			Spessartine			Uvarovite			Almandine		
	$\overline{v}_p$	$\overline{v}_s$	A	$\overline{v}_p$	$\overline{v}_s$	A	$\overline{v}_p$	$\overline{v}_s$	A	$\overline{v}_p$	$\overline{v}_s$	A	$\overline{v}_p$	$\overline{v}_s$	A	$\overline{v}_p$	$\overline{v}_s$	A
0	9.182	5.118	-3.0	9.495	5.572	-5.6	8.504	4.866	-10.0	8.664	4.839	-2.5	8.762	5.087	-15.8	8.502	4.683	-4.5
4	9.397	5.208	-2.2	9.727	5.641	-7.4	8.759	4.932	-11.7	8.881	4.907	-3.6	8.993	5.127	-16.6	8.760	4.794	-4.1
8	9.712	5.345	-2.0	9.938	5.697	-9.1	8.988	4.981	-12.9	9.079	4.964	-4.1	9.204	5.158	-16.9			
12	9.936	5.422	-1.6	10.128	5.749	-10.0	9.198	5.021	-13.4	9.267	5.014	-4.5	9.401	5.184	-17.1			
20	10.324	5.535	-1.2	10.474	5.805	-11.7	9.520	5.060	-14.0	9.605	5.090	-5.1	9.697	5.194	-16.9			
30	10.742	5.638	-1.9	10.848	5.855	-12.5	9.891	5.090	-14.4	9.969	5.153	-5.1	10.044	5.194	-16.5			
40	11.100	5.708	-0.4	11.167	5.881	-13.2	10.207	5.094	-14.5	10.294	5.201	-5.1						
60	11.704	5.798	+0.3	11.683	5.890	-13.0												

(the reader can find the explicit values of the computed densities in Table II of Ref. 6). Another consideration that can be made from the analysis of Figure 3 is that seismic wave velocities increase as pressure increases.

From directional seismic wave velocities, the elastic anisotropy of a crystal can be fully characterized. The azimuthal anisotropy for quasi-longitudinal and quasi-transverse seismic wave velocities can be defined as follows:[28]

$$A_X = \frac{v_{X_{max}} - v_{X_{min}}}{\overline{v}_X} \, , \qquad (10)$$

where $X = p, s$ labels longitudinal and shear waves and $\overline{v}_X$ is the polycrystalline isotropic average velocity obtained from Voigt-Reuss-Hill scheme, whose expression is given in equation (8). Elastic anisotropy would be zero for an ideal isotropic material; even cubic crystals, such as silicate garnets, however, show a non-zero elastic anisotropy.[28] For cubic crystals, the elastic anisotropy can be given a simple expression in terms of a single anisotropy index computed from the elastic constants:[75]

$$A = \left(\frac{2B_{44} + B_{12}}{B_{11}} - 1 \right) \times 100 \, . \qquad (11)$$

Computed average isotropic seismic wave velocities (longitudinal $\overline{v}_p$ and shear $\overline{v}_s$) and elastic anisotropy index A are reported in Table II as a function of pressure for the six end-members. In the absence of external pressure, the six silicate garnet end-members can be sorted in terms of increasing elastic anisotropy, as follows: Spe $<$ Pyr $<$ Alm $<$ Gro $<$ And $\ll$ Uva. Spessartine and pyrope show very low anisotropy while uvarovite is by far the most anisotropic among them.

Let us analyze the effect of pressure on the elastic anisotropy of this class of materials. From Figure 3 and Table II it is seen that the elastic anisotropy of grossular, uvarovite, spessartine and andradite increases as a function of pressure. In particular, grossular and spessartine are the most affected by pressure, with anisotropies varying from -5.6 % to -13.2 % and from -2.5 % to -5.1 %, respectively, when passing from 0 GPa to 40 GPa; the elastic anisotropy of andradite increases form -10 % to -14.5 % in the same pressure range while the anisotropy of uvarovite only slightly increases form -15.8 % to -16.5 % passing from 0 GPa up to 30 GPa. Pyrope and almandine show a different behavior under pressure: their elastic anisotropy decreases. If at ambient pressure pyrope shows a larger anisotropy than spessartine, as soon as pressure increases the anisotropy of spessartine becomes larger than pyrope.

V. CONCLUSIONS

A general *ab initio* methodology has been devised and implemented in the CRYSTAL program for analyzing the evolution under pressure of the elastic anisotropy of crystalline materials. The scheme, developed within periodic boundary conditions, localized atomic orbitals and one-electron Hamiltonians, has been applied to a family of silicate garnets which are among the main rock-forming minerals of the Earth's mantle. The characterization of the elastic anisotropy of minerals is of particular interest

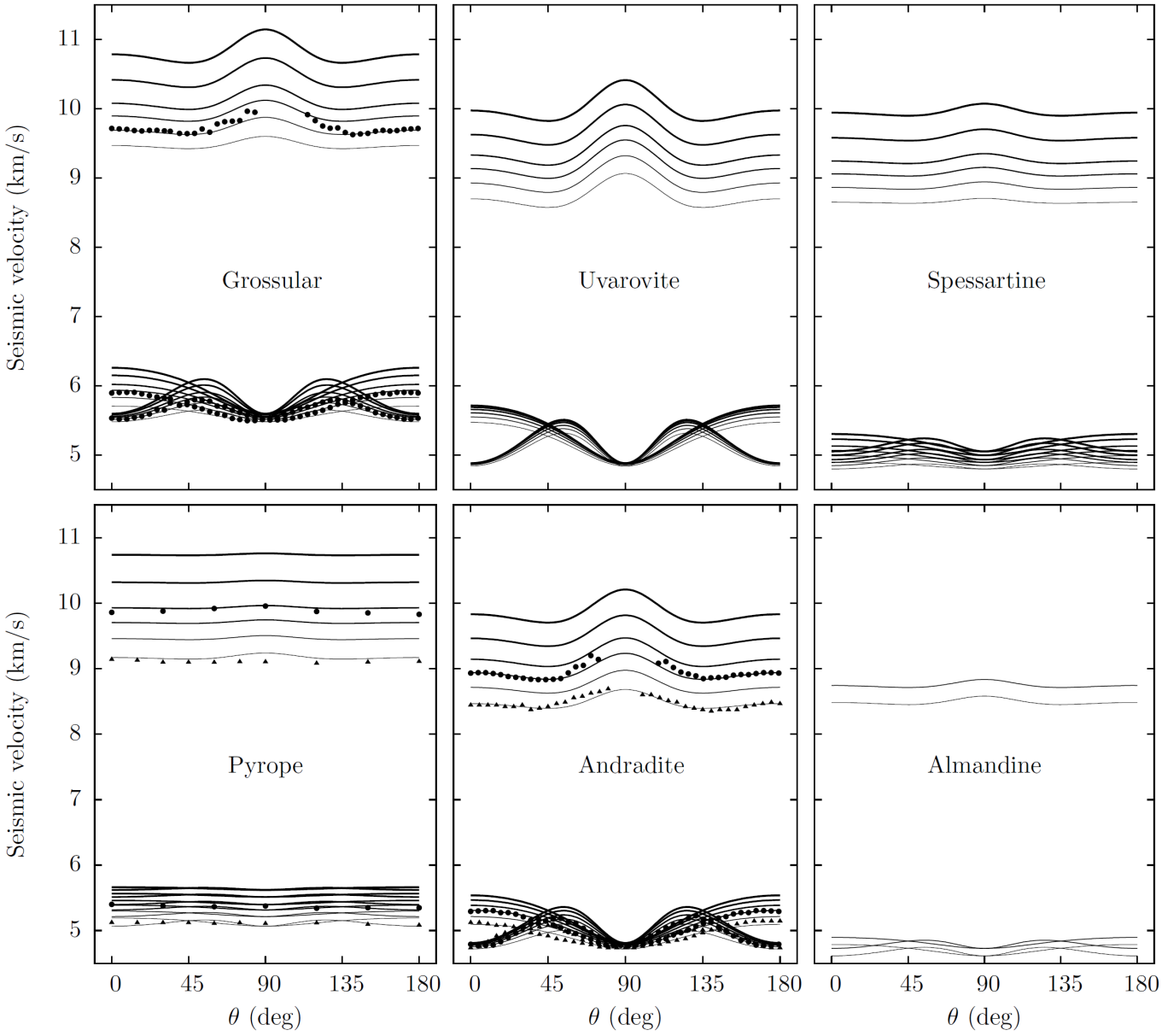

FIG. 3. Directional quasi-transverse and quasi-longitudinal seismic wave velocities of single-crystal grossular, uvarovite, spessartine, pyrope, andradite and almandine along an azimuthal angle θ (defined in the text). Computed data at different pressures (0 GPa, 4 GPa, 8 GPa, 12 GPa, 20 GPa, 30 GPa) are reported as continuous lines of increasing thickness. Experimental data by Jiang *et al.*[25] for andradite at ambient pressure (triangles), downshifted by 0.1 km/s, and at 8.7 GPa (circles) are reported. Experimental data by Jiang *et al.*[67] for a grossular-rich garnet at 4.3 GPa (circles) are also reported, downshifted by 0.4 km/s for quasi-longitudinal and 0.24 km/s for quasi-transverse seismic wave velocities. For pyrope, data by Sinogeikin and Bass[15] are reported at 0 GPa (triangles) and 13.9 GPa (circles).

to the geophysical description of the Earth's deep interior and to the understanding of seismic wave propagation during earthquakes.

The elastic properties under geophysical pressure of spessartine, uvarovite and almandine have been investigated with an *ab initio* technique for the first time. Furthermore, azimuthal anisotropy and shear-wave birefringence of seismic velocities have been fully characterized for the six silicate garnet end-members as a function of increasing pressure, up to 60 GPa. The propagation velocity of elastic waves has been found to systematically increase with pressure. The evolution of elastic anisotropy with pressure has also been investigated. Pyrope and almandine have been found to decrease their

elastic anisotropy with pressure while for grossular, andradite, spessartine and uvarovite it increases, more so for grossular and spessartine than for andradite and uvarovite.

ACKNOWLEDGMENTS

The authors want to express their gratitude to Dr. Elisa Albanese for her contribution to the implementation of Christoffel's equation in the CRYSTAL program. Improvements of the CRYSTAL code in its massive-parallel version were made possible thanks to the PRACE proposal no. 2011050810.

[1] D. L. Anderson, *Theory of the Earth* (Blackwell Scientific Publications, Boston, 1989).
[2] P. C. Rickwood, M. Mathias, and J. C. Siebert, Contrib. Mineral. Petrol. **19**, 271 (1968).
[3] A. E. Ringwood, *Composition and Petrology of the Earth's Mantle* (McGraw-Hill, New York, 1975).
[4] J. D. Bass and D. L. Anderson, Geophys. Res. Lett. **11**, 229 (1984).
[5] D. L. Anderson and J. D. Bass, Nature **320**, 321 (1986).
[6] A. Erba, A. Mahmoud, R. Orlando, and R. Dovesi, Phys. Chem. Minerals **41**, 151 (2014).
[7] A. Erba, A. Mahmoud, R. Orlando, and R. Dovesi, Phys. Chem. Minerals **41**, 161 (2014).
[8] A. Erba, A. Mahmoud, D. Belmonte, and R. Dovesi, J. Chem. Phys. **140**, 124703 (2014).
[9] V. Lacivita, A. Erba, R. Dovesi, and P. D'Arco, J. Chem. Phys. (2014), in preparation.
[10] D. G. Isaak and E. K. Graham, J. Geophys. Res. **81**, 2483 (1976).
[11] L. J. Bonczar, E. K. Graham, and H. Wang, J. Geophys. Res. **82**, 2529 (1977).
[12] B. J. Leitner, D. J. Weidner, and R. C. Liebermann, Phys. Earth Planet. Int. **22**, 111 (1980).
[13] B. O'Neill, J. D. Bass, J. R. Smyth, and M. T. Vaughan, J. Geophys. Res. **94**, 17819 (1989).
[14] B. O'Neill, J. D. Bass, G. R. Rossman, C. A. Geiger, and K. Langer, Phys. Chem. Miner. **17**, 617 (1991).
[15] S. V. Sinogeikin and J. D. Bass, Phys. Earth Planet. Int. **120**, 43 (2000).
[16] T. S. Duffy and D. L. Anderson, J. Geophys. Res. **94**, 1895 (1989).
[17] G. Chen, J. A. Cooke, G. D. Gwanmesia, and R. C. Liebermann, Am. Miner. **84**, 384 (1999).
[18] A. Chopelas, H. J. Reichmann, and L. Zhang, in *Mineral Spectroscopy*, edited by M. D. Dyar, C. McCammon, and M. W. Schaefer (Geochem. Soc., Washington, D.C., 1996), p. 229.
[19] Z. Wang and S. Ji, Am. Miner. **86**, 1209 (2001).
[20] C. Lu, Z. Mao, J.-F. Lin, K. K. Zhuravlev, S. N. Tkachev, and V. B. Prakapenka, Earth and Planetary Science Letters **361**, 134 (2013).
[21] J. D. Bass, J. Geophys. Res. **94**, 7621 (1989).
[22] Y. Sumino and L. O. Anderson, in *Handbook of Physical Properties of Rocks*, edited by R. S. Carmichael (CRC Press, Boca Raton, Florida, 1982), p. 39.
[23] P. M. Halleck, Ph.D. dissertation p. 82 (1973).
[24] J. D. Bass, J. Geophys. Res. **91**, 7505 (1986).
[25] F. Jiang, S. Speziale, S. R. Shieh, and T. S. Duffy, J. Phys.:Condens. Matter **16**, S1041 (2004).
[26] M. J. P. Musgrave, *Crystal Acoustics* (Holden-Day, San Francisco, California, 1970).
[27] B. A. Auld, *Acoustic Fields and Waves in Solids* (Krieger Publishing Company, Malabar, Florida, 1973).
[28] B. B. Karki, L. Stixrude, and R. M. Wentzcovitch, Rev. Geophys. **39**, 507 (2001).
[29] R. Dovesi, V. R. Saunders, C. Roetti, R. Orlando, C. M. Zicovich-Wilson, F. Pascale, K. Doll, N. M. Harrison, B. Civalleri, I. J. Bush, et al., *CRYSTAL14 User's Manual*, Università di Torino, Torino (2013), http://www.crystal.unito.it.
[30] R. Dovesi, R. Orlando, A. Erba, C. M. Zicovich-Wilson, B. Civalleri, S. Casassa, L. Maschio, M. Ferrabone, M. De la Pierre, P. D'Arco, et al., Int. J. Quantum Chem. (2014), dOI:10.1002/qua.24658.
[31] A. Erba, M. Ferrabone, J. Baima, R. Orlando, M. Rérat, and R. Dovesi, J. Chem. Phys. **138**, 054906 (2013).
[32] V. Lacivita, A. Erba, Y. Noël, R. Orlando, P. D'Arco, and R. Dovesi, J. Chem. Phys. **138**, 214706 (2013).
[33] A. Erba, K. E. El-Kelany, M. Ferrero, I. Baraille, and M. Rérat, Phys. Rev. B **88**, 035102 (2013).
[34] J. Baima, A. Erba, R. Orlando, M. Rérat, and R. Dovesi, J. Phys. Chem. C **117**, 12864 (2013).
[35] A. Erba and R. Dovesi, Phys. Rev. B **88**, 045121 (2013).
[36] A. Mahmoud, A. Erba, K. E. El-Kelany, M. Rérat, and R. Orlando, Phys. Rev. B **89**, 045103 (2014).
[37] A. D. Becke, J. Chem. Phys. **98**, 5648 (1993).
[38] C. Lee, W. Yang, and R. G. Parr, Phys. Rev. B **37**, 785 (1988).
[39] K. Doll, R. Dovesi, and R. Orlando, Theor. Chem. Acc. **112**, 394 (2004).
[40] K. Doll, R. Dovesi, and R. Orlando, Theor. Chem. Acc. **115**, 354 (2006).
[41] K. Doll, Molecular Physics **108**, 223 (2010).
[42] W. F. Perger, J. Criswell, B. Civalleri, and R. Dovesi, Comput. Phys. Commun. **180**, 1753 (2009).
[43] B. B. Karki, G. J. Ackland, and J. Crain, J. Phys.: Cond. Matter **9**, 8579 (1997).
[44] J. Wang, J. Li, S. Yip, S. Phillpot, and D. Wolf, Phys. Rev. B **52**, 12627 (1995).
[45] D. C. Wallace, *Thermodynamics of Crystals* (Wiley, New York, USA, 1972).
[46] D. C. Wallace, Rev. Mod. Phys. **37**, 57 (1965).
[47] J. F. Nye, *Physical properties of crystals* (Oxford University Press, Oxford, 1957).
[48] C. M. Zicovich-Wilson, F. J. Torres, F. Pascale, L. Valenzano, R. Orlando, and R. Dovesi, J. Comput. Chem. **29**, 2268 (2008).
[49] F. Pascale, C. Zicovich-Wilson, R. Orlando, C. Roetti, P. Ugliengo, and R. Dovesi, J. Phys. Chem. B **109**, 6146 (2005).
[50] R. Dovesi, M. De La Pierre, A. M. Ferrari, F. Pascale, L. Maschio, and C. M. Zicovich-Wilson, Am. Mineral. **96**, 1787 (2011).
[51] K. Doll, Comput. Phys. Commun. **137**, 74 (2001).
[52] K. Doll, V. Saunders, and N. Harrison, Int. J. Quantum Chem. **82**, 1 (2001).
[53] B. Civalleri, P. D'Arco, R. Orlando, and R. D. V. R. Saunders, Chem. Phys. Lett. **348**, 131 (2001).
[54] C. G. Broyden, J. Inst. Math. Appl. **6**, 76 (1970).
[55] R. Fletcher, Comput. J **13**, 317 (1970).
[56] D. Goldfarb, Math. Comput. **24**, 23 (1970).
[57] D. F. Shanno, Math. Comput. **24**, 647 (1970).
[58] L. Zhang, H. Ahsbahs, and A. Kutoglu, Phys. Chem. Minerals **25**, 301 (1998).
[59] L. Zhang, H. Ahsbahs, A. Kutoglu, and C. A. Geiger, Phys. Chem. Minerals **27**, 52 (1999).
[60] F. D. Murnaghan, Proc. Natl. Acad. Sci. USA **30**, 244 (1944).
[61] F. Birch, Phys. Rev. **71**, 809 (1947).
[62] J.-P. Poirier and A. Tarantola, Physics of the Earth and Planetary Interiors **109**, 1 (1998).
[63] P. Vinet, J. Ferrante, J. H. Rose, and J. R. Smith, J. Geophys. Res.: Solid Earth **92**, 9319 (1987).
[64] V. Diella, A. Sani, D. Levy, and A. Pavese, Am. Mineral **89**, 371 (2004).
[65] J. M. Leger, A. M. Redon, and C. Chateau, Phys. Chem. Minerals **17**, 161 (1990).
[66] S. Gréaux and A. Yamada, Phys. Chem. Minerals **41**, 141 (2012).
[67] F. Jiang, S. Speziale, and T. S. Duffy, J. Geophys. Res. **109**, B10210 (2004).
[68] R. Hill, J. Mech. Phys. Solids **11**, 357 (1963).

[69] R. Hill, Proc. Phys. Soc. A **65**, 349 (1952).
[70] G. D. Gwanmesia, J. Zhang, K. Darling, J. Kung, B. Li, L. Wang, D. Neuville, and R. C. Liebermann, Phys. Earth Planet. Inter. **155**, 179 (2006).
[71] X. Q. Chen, C. L. Fu, and R. Podloucky, Phys. Rev. B **77**, 064103 (2008).
[72] G. D. Gwanmesia, L. Wang, A. Heady, and R. C. Liebermann, Phys. Earth Planet. Inter. **228**, 80 (2014).
[73] Y. Kono, S. Gréaux, Y. Higo, H. Ohfuji, and T. Irifune, J. Earth Sci. **21**, 782 (2010).
[74] G. Ottonello, B. Civalleri, J. Ganguly, W. F. Perger, D. Belmonte, and M. Vetuschi Zuccolini, Am. Mineral. **95**, 563 (2010).
[75] A. Authier and A. Zarembowitch, in *International Tables for Crystallography, Vol. D*, edited by A. Authier (Wiley, 2006), p. 72.